Available online at www.sciencedirect.com
ScienceDirect
Trans. Nonferrous Met. Soc. China 26(2016) 2390−2396
Transactions of Nonferrous Metals Society of China
www.tnmsc.cn

Photoelectrocatalytic reduction of CO_2 into formic acid using WO_{3-x}/TiO_2 film as novel photoanode

Ya-hui YANG[1], Ren-rui XIE[1], Hang LI[1], Can-jun LIU[2], Wen-hua LIU[2], Fa-qi ZHAN[2]

1. College of Resources and Environment, Hunan Agricultural University, Changsha 410128, China;
2. School of Chemistry and Chemical Engineering, Central South University, Changsha 410083, China

Received 11 June 2016; accepted 1 September 2016

Abstract: A novel WO_{3-x}/TiO_2 film as photoanode was synthesized for photoelectrocatalytic (PEC) reduction of CO_2 into formic acid (HCOOH). The films prepared by doctor blade method were characterized with X-ray diffractometer (XRD), scanning electron microscope (SEM) and transmission electron microscope (TEM). The existence of oxygen vacancies in the WO_{3-x} was confirmed with an X-ray photoelectron spectroscopy (XPS), and the accurate oxygen index was determined by a modified potentiometric titrimetry method. After 3 h of photoelectrocatalytic reduction, the formic acid yield of the WO_{3-x}/TiO_2 film is 872 nmol/cm^2, which is 1.83 times that of the WO_3/TiO_2 film. The results of PEC performance demonstrate that the introduction of WO_{3-x} nanoparticles can improve the charge transfer performance so as to enhance the performance of PEC reduction of CO_2 into formic acid.
Key words: photoelectrocatalytic reduction; CO_2; formic acid; WO_{3-x}; TiO_2; film photoanode

1 Introduction

The global warming and depletion of fossil fuels are two major problems that mankind is facing today [1−3]. Photoelectrocatalytic (PEC) or photocatalytic (PC) reduction of CO_2 to fuel is considered an ideal and practical solution to the problems, as it utilizes solar energy and H_2O for the reduction of CO_2 in a similar way to natural photosynthesis without pollutants [4−6]. And the fuel as product can be used in the internal combustion engine or as chemical feedstock.

An ideal photocatalyst for CO_2 reduction should be environmentally friendly. More importantly, it should have a suitable band structure for reducing CO_2 and oxidizing water simultaneously [7,8]. However, the efficiency of reducing CO_2 has been limited by the recombination of the photogenerated charge carriers. Recently, a photoanode-driven PEC system for conversion of CO_2 to fuels has attracted much attention because it can supply the additional energy to reduce CO_2 and oxidize H_2O with decreased charge recombination [1,9]. Among various photoanode materials, TiO_2 is widely used for CO_2 photoreduction due to its low toxicity, inexpensive and photocorrosion resistance [5, 10]. To improve the photocatalytic activity of TiO_2 based photoanode, many research efforts have been done such as doping with metals and mixing with other metal oxides [11−16].

Tungsten oxide (WO_3) with a band gap of about 2.7 eV has been widely utilized to couple with TiO_2 [17,18]. This is mainly because WO_3 can serve as a coupling agent with TiO_2 to facilitate charge separation and mobility. Similar strategy can be applied in the TiO_2 based dye-sensitized solar cells (DSSCs) [19]. More interestingly, non-stoichiometric tungsten oxide with oxygen deficiency (WO_{3-x}) has a higher electron mobility (10−20 $cm^2 \cdot V^{-1} \cdot s^{-1}$) [20,21] and can be widely used as electron-selective materials in solar cells [22,23]. Considering the unsatisfactory efficiency of photoelectrocatalytic CO_2 reduction by the TiO_2 photoanode, combining TiO_2 with WO_{3-x} may provide a strategy to improve the seperation of photo-generated electrons and holes. To the best of our knowledge, no such constructed photoanode has been used to photoelectrocatalytic reduction of CO_2.

In this work, we fabricated a novel WO_{3-x}/TiO_2 film photoanode by the doctor blading method at low temperature. The introduction of WO_{3-x} improved the rate of electron transfer and suppressed recombination synergistically, resulting in an improvement in the performance of PEC reducing CO_2 into formic acid. In

Foundation item: Project (21471054) supported by the National Natural Science Foundation of China
Corresponding author: Ya-hui YANG; Tel: +86-731-84617670; E-mail: yangyahui2002@sina.com
DOI: 10.1016/S1003-6326(16)64376-5

order to better understand the improved reason, the PEC performance has been investigated by photocurrent and electrochemical impedance measurements.

2 Experimental

2.1 Materials

TiO_2 nanoparticles (Degussa P25, Germany), ammonium metatungstate ($(NH_4)_6H_2W_{12}O_4{\cdot}xH_2O$, 99.99%, Aladdin), polyvinylpyrrolidone (PVP, 99.99%, Aladdin), polyethylene glycol (PEG1000, 99.99%, Aladdin) were used as-received. The fluorine-doped SnO_2 glass (FTO) as the substrate of film was purchased from NSG Corporation.

2.2 Synthesis of WO_{3-x} nanoparticles

The WO_3 nanoparticles were prepared by a solution method according to our previous work [24]. 2 g of PVP was dissolved in 15 mL of deionized (DI) water. $(NH_4)_6H_2W_{12}O_4{\cdot}xH_2O$ (1.478 g) was suspended in 10 mL of DI water and then dropped into the above PVP solution with continual stirring. After 30 min of ultrasonic treating and 2 h of stirring, 2.000 g of PEG1000 was added in it with continual stirring for additional 4 h. The as-prepared precursor was completely dried at 80 °C, followed by sintering at 600 °C for 1 h.

The WO_{3-x} nanoparticles were prepared by a hydrogen reduction method. In a typical experiment, 1 g of WO_3 nanoparticles was calcined in reducing gas (V(Ar):V(H_2)=95:5) at the flow rate of 0.2 L/min and 400 °C for 2 h.

2.3 Preparation of TiO_2/WO_{3-x} films

The TiO_2/WO_{3-x} film was prepared by using a doctor-blade technique. In detail, 0.285 g P25, 0.015 g WO_{3-x} nanoparticles, 1.585 mL ethyl alcohol and 0.415 mL dilute HCl solution (pH≈4) were added to an agate jar. The TiO_2/WO_{3-x} paste can be obtained by ball milling for 2 h. The prepared paste was coated on the FTO substrate by a doctor-blade coater and then dried at 60 °C for 60 min. Finally, the as-prepared film was baked at 120 °C for 15 min.

2.4 Characterization

The crystalline phase of the samples was characterized with an X-ray diffractometer (XRD, D/Max2250, Rigaku Corporation, Japan) at a scanning speed of 8 (°)/min. The surface morphology and microstructure of the sample were investigated with a field emission scanning electron microscope (FESEM, NanoSEM 230) coupled with energy dispersive X-ray spectroscopy (EDS) and a transmission electron microscope (TEM, TECNAI G2 F20, FEI). EDS was used to analyse the elements of as-prepared sample. The chemical composition of the sample was analyzed with an X-ray photoelectron spectroscope (XPS, K-Alpha 1063, Thermo Fisher Scientific). The absorbance of photoanodes were performed through a diffuse reflectance ultraviolet and visible spectrophotometer (UV-Vis Pgeneral TU-1901).

2.5 Determination of oxygen index

The oxygen index was determinated by a modified method of potentiometric titrimetry [25−27]. In details, 0.200 g WO_{3-x} powder was put in a 250 mL conical flask. 5 mL of 0.2 mol/L $K_3[Fe(CN)_6]$ and 15 mL of 1 g/L KOH solution were added. The mixture was heated in an oven at 70 °C for 15 min to dissolve WO_{3-x} powder, and then naturally cooled to room temperature. After that, 10 mL of concentrated hydrochloric acid, 10 mL of DI water and 20 mL of 10 g/L KI solution were injected. The potentiometric titrimetry was carried out in a two electrode configuration in which Pt plate and Ag/AgCl/satd. KCl were used as work electrode and counter/reference electrodes, respectively, and the above solution was used as electrolyte. Under continuous stirring, it was titrated with a standard solution of $Na_2S_2O_3$ (0.05 mol/L). The titration was terminated when an obvious potential change happens, and the consumption of $Na_2S_2O_3$ is V_1. In addition, a coefficient $K=G_2/G_1$ was also gained, where G_1 is the mass of sample before annealing, and G_2 is the mass of sample after annealing at 400 °C for 30 min in air. Finally, the oxygen index (3−x) of non-stoichiometric tungsten oxides was calculated based on the following equation:

$$(3-x)=3-\frac{0.1159\times(0.2\times5-0.05\times V_1)}{0.200\times K} \quad (1)$$

and the oxygen index in this experiment is 2.65.

2.6 Photoelectrochemical measurements

The photoelectrochemical experiments were carried out using an electrochemical analyzer (Zennium, Zahner, Germany) with a three electrode quartz cell that includes a work electrode, a platinum or copper electrode and an Ag/AgCl/satd. KCl reference electrode. A 500 W Xe lamp adjusted to 100 mW/cm^2 (CHF-XM35, Beijing Trusttech Co. Ltd.) was used as the light source. For photoelectrochemical measurements, the electrodes were immersed in 0.2 mol/L Na_2SO_4 solution and the scanning rate of cyclic voltammetry is 20 mV/s. The electrochemical impedance spectra were measured at the potential of 0.8 V (vs Ag/AgCl) with a 10 mV AC voltage perturbation and the range of frequency is 10000 to 0.1 Hz. For the experiment of reducing CO_2, the reactor with a Nafion membrane has two compartments for water oxidation (anodic) and CO_2 reduction (cathodic), respectively. In the cell for water oxidation,

the as-prepared film, Ag/AgCl and 0.2 mol/L Na_2SO_4 solution were used as photoanode, reference electrode and electrolyte, respectively. In the compartment for CO_2 reduction, the copper electrode and 0.5 mol/L $KHCO_3$ solution were used as cathode and electrolyte, respectively. A constant potential of 1.2 V (vs Ag/AgCl) was applied for CO_2 reduction. The CO_2 gas was injected during the whole test process. The formic acid in the electrolyte was analyzed by headspace method using a gas chromatograph-mass spectrometer (ICS 2000, Dionex, USA).

3 Result and discussion

3.1 Morphology and structure

The morphology of WO_{3-x} nanoparticle was investigated using FESEM. Figure 1(a) shows the morphology of WO_{3-x} nanoparticles. As shown in Fig. 1(a), all the WO_{3-x} nanoparticles exhibit the morphology of spherical particles with a diameter of 30−80 nm. The XRD pattern of WO_{3-x} nanoparticles is shown in Fig. 1(b). The diffraction peaks of WO_{3-x} nanoparticles at 23.0°, 23.5°, 24.3°, 26.5°, 28.7°, 33.1°, 33.8°, 35.4°, 41.6°, 47.0°, 48.1°, 49.9° and 55.7° are in accordance with (002), (020), (200), (120), (112), (022), (202), (122), (222), (004), (040), (232) and (402) planes of tungsten oxide, which can be indexed to WO_3 (JCPDS No. 89-7796).

In order to better observe the particle size and crystal structure of WO_3 and WO_{3-x} nanoparticles, the TEM images of WO_3 and WO_{3-x} nanoparticles are shown in Fig. 2. Figures 2(a) and (b) show the low resolution

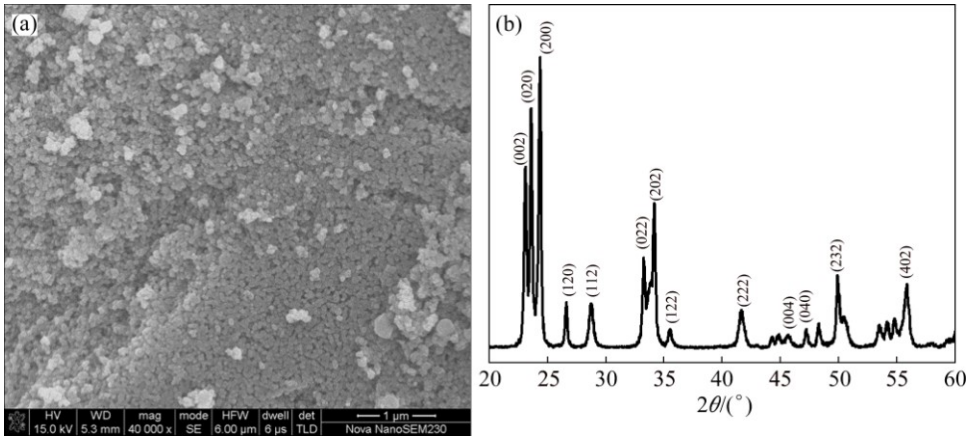


Fig. 1 SEM image (a) and XRD pattern (b) of WO_{3-x} nanoparticles

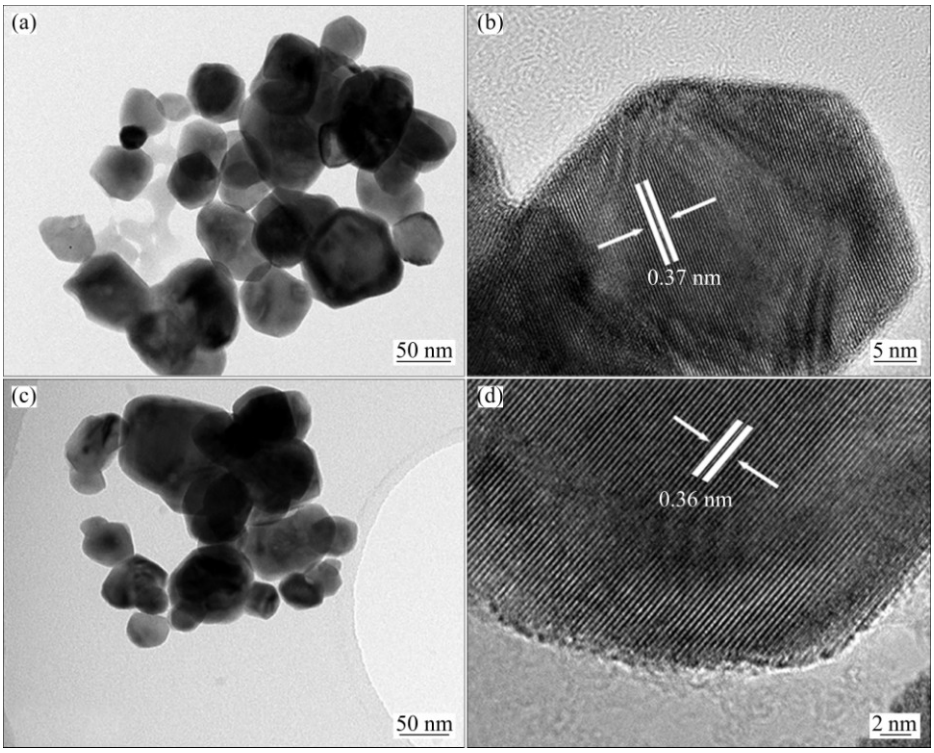
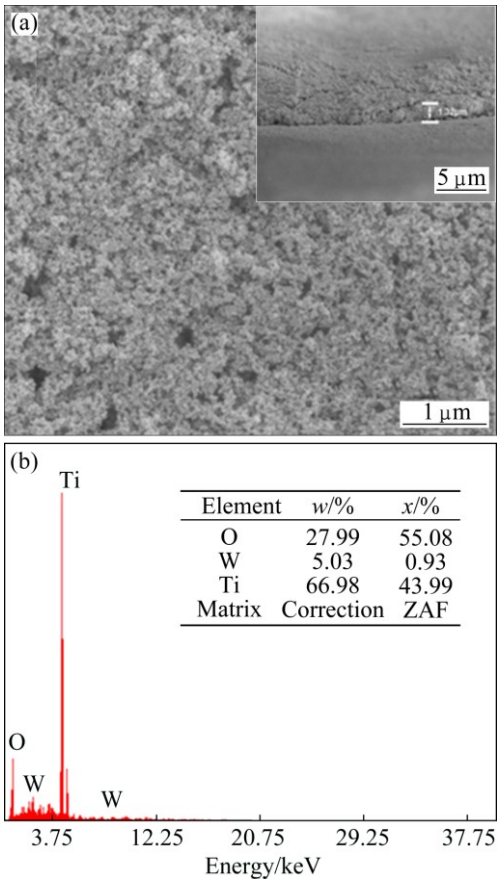


Fig. 2 TEM images of WO_3 (a, b) and WO_{3-x} (c, d) nanoparticles

and high resolution TEM images of WO_3 nanoparticles, respectively. As shown in Fig. 2(a), the size of WO_3 nanoparticles is 30−80 nm. The observed lattice fringes of 0.36 nm in Fig. 2(b) corresponds to the (002) plane of monoclinic WO_3 (JCPDS No. 89-7796). The TEM images of WO_{3-x} nanoparticles are shown in Figs. 2(c) and (d). It can be seen from Fig. 2(c) that the particle size of WO_{3-x} nanoparticle is similar to that of WO_3 nanoparticle. The interplanar spacing is 0.36 nm, which is consistent with the (200) plane of monoclinic WO_3 (JCPDS No. 89-7796). The TEM results indicate that there is almost no change in the particle size and crystal structure of WO_3 nanoparticles after H_2-treatment.

Figure 3(a) shows the FESEM image of WO_{3-x}/TiO_2 films. As shown in Fig. 3(a), the WO_{3-x}/TiO_2 film is composed of uniform nanoparticles with a thickness of 1 μm. The local composition of WO_{3-x}/TiO_2 film was analyzed with an EDS spectrometer. The EDS result (Fig. 3(b)) indicates the existence of O, W and Ti.



Element	w/%	x/%
O	27.99	55.08
W	5.03	0.93
Ti	66.98	43.99
Matrix	Correction	ZAF

Fig. 3 FESEM image (a) and EDS pattern (b) of WO_{3-x}/TiO_2 film

The crystallographic structure and phase purity of TiO_2, WO_3/TiO_2, and WO_{3-x}/TiO_2 films were examined by XRD analysis and the results are shown in Fig. 4. The XRD patterns of the three films present the same peaks, corresponding to rutile TiO_2 (JCPDS No. 73-2224) and FTO substrate (SnO_2, JCPDS No. 71-0652), and no other obvious peaks can be observed in all patterns, which are likely due to low WO_3 and WO_{3-x} content.

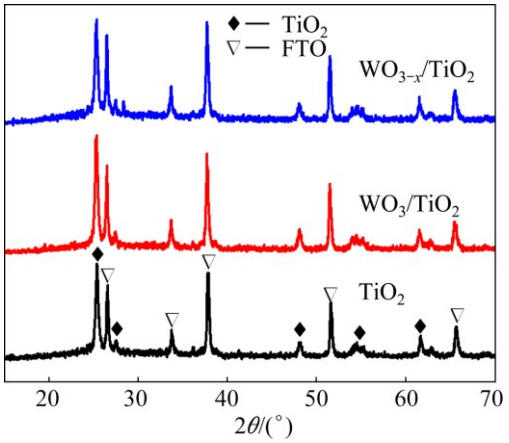


Fig. 4 XRD patterns of TiO_2, WO_3/TiO_2, and WO_{3-x}/TiO_2 films

3.2 Chemical composition of WO_{3-x}

To confirm the existence of oxygen vacancies, the chemical states of O and W in the WO_{3-x} nanoparticles were studied by XPS. The XPS spectra have been fitted by the Gaussian-Lorentzian function. The O 1s and W 4f XPS spectra of WO_{3-x} are shown in Fig. 5. In Fig. 5, the characteristic peaks at 530.5 and 531.2 eV are attributed to O^{2-} and O^-, respectively [28,29]. For the W 4f XPS

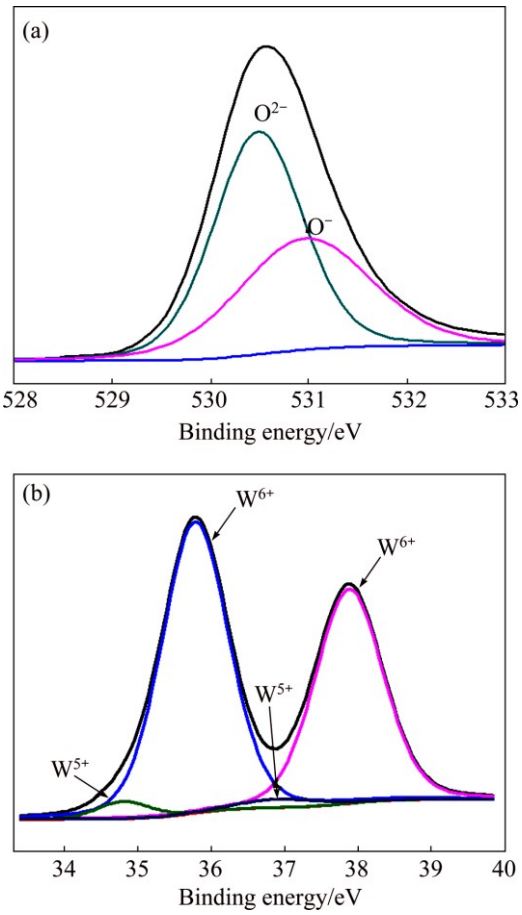


Fig. 5 XPS spectra of WO_{3-x}: (a) O 1s; (b) W 4f

spectrum, the separated peaks centered at the binding energies of 34.8 and 36.9 eV correspond to the typical binding energies of W^{5+} [30]. This confirms that oxygen vacancies and W^{5+} are created after H_2-treatment.

3.3 Optical properties

The light absorption spectra of all films are presented in Fig. 6. The pure TiO_2 film exhibits an absorption edge of ~400 nm. With the introduction of WO_3 and oxygen vacancies (WO_{3-x}), a high absorbance in the visible region is obtained.

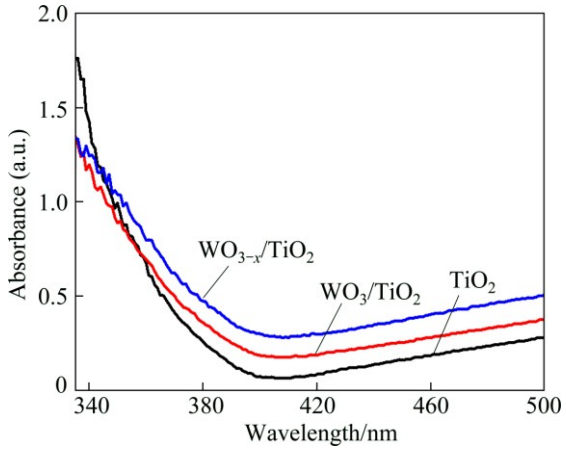


Fig. 6 UV-Vis spectra of TiO_2, WO_3/TiO_2, and WO_{3-x}/TiO_2 films

3.4 Photoelectrochemical performance

The PEC CO_2 reduction experiments were carried out under irradiation of a 500 W Xe lamp with a power density of 100 mW/cm^2, and the formic acid in solution was analyzed with a gas chromatograph-mass spectrometer (GC-MS). After 3 h of photoelectrocatalytic reduction, the production yields of HCOOH for TiO_2, WO_3/TiO_2 and WO_{3-x}/TiO_2 films were recorded as shown in Fig. 7. Compared with the pure TiO_2 film (335 nmol/cm^2), the WO_3/TiO_2 film exhibits an enhanced production yield of HCOOH (475 nmol/cm^2), which is because the improved separation of photon-generated carrier by the introduction of WO_3 [19,31]. Particularly, the production yield of WO_{3-x}/TiO_2 film is 872 nmol/cm^2, which is 1.83 times that of WO_3/TiO_2 film. This indicates that the WO_{3-x}/TiO_2 film has a good ability for the PEC CO_2 reduction.

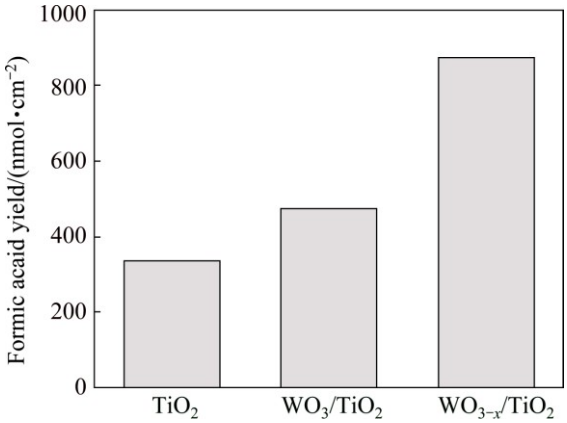


Fig. 7 Formic acid yields for TiO_2, WO_3/TiO_2 and WO_{3-x}/TiO_2 film after 3 h of photoelectrocatalytic reduction

To better understand the enhanced performance of PEC CO_2 reduction for WO_{3-x}/TiO_2 film, TiO_2, WO_3/TiO_2 and WO_{3-x}/TiO_2 films were used as photoanodes in a typical PEC cell, and their PEC performance was investigated in 0.2 mol/L Na_2SO_4 and 0.5 mol/L $NaHCO_3$ solution. Figure 8(a) shows the photocurrent density plots of TiO_2, WO_3/TiO_2 and WO_{3-x}/TiO_2 films. The WO_3/TiO_2 film exhibits a higher photocurrent density than the pure TiO_2 electrode. Importantly, the photocurrent density of WO_{3-x}/TiO_2 film is larger than that of the WO_3/TiO_2 film. It agrees with the performance of PEC CO_2 reduction for the three films. Figure 8(b) shows the electrochemical impedance spectroscopy (EIS) of TiO_2, WO_3/TiO_2 and WO_{3-x}/TiO_2 films at the applied potential of 0.8 V (vs Ag/AgCl) under illumination conditions. The EIS analysis is a very useful tool to study the electron transport property of film photoelectrode. In EIS Nyquist plot, a smaller circular radius means lower charge transfer resistance in the electrode [32−34]. As shown in Fig. 8(b), the EIS Nyquist plot of WO_{3-x}/TiO_2 film exhibits the smallest circular radius among the three films, suggesting the

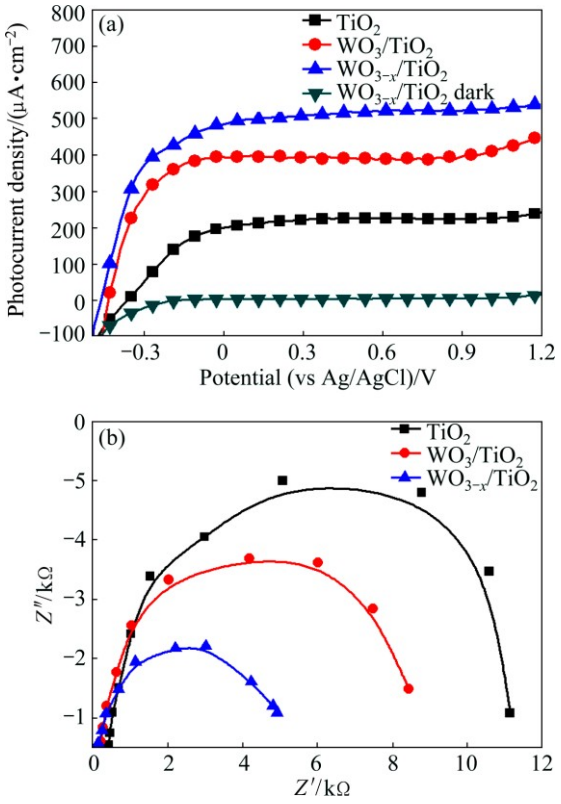


Fig. 8 Photocurrent density (a) and EIS (b) plots of TiO_2, WO_3/TiO_2 and WO_{3-x}/TiO_2 films

lowest charge transfer resistance in WO_{3-x}/TiO_2 film. This may be a probable explanation why the WO_{3-x}/TiO_2 film exhibits a better performance of PEC CO_2 reduction.

4 Conclusions

1) A novel WO_{3-x}/TiO_2 photoanode was fabricated by a hydrogen reduction method and low temperature doctor blade technique.

2) After 3 h of photoelectrocatalytic reduction, the formic acid yield of the WO_{3-x}/TiO_2 film is 872 nmol/cm^2, which is 1.83 times that of the WO_3/TiO_2 film.

3) The introduction of WO_{3-x} nanoparticles reduces the charge transfer resistance, resulting in an improved performance of PEC CO_2 reduction for the WO_{3-x}/TiO_2 film.

References

[1] MAGESH G, KIM E S, KANG H J, BANU M, KIM J Y, KIM J H, LEE J S. A versatile photoanode-driven photoelectrochemical system for conversion of CO_2 to fuels with high faradaic efficiencies at low bias potentials [J]. Journal of Materials Chemistry A, 2014, 2(7): 2044−2049.

[2] IBRAHIM N, KAMARUDIN S K, MINGGU L. Biofuel from biomass via photo-electrochemical reactions: An overview [J]. Journal of Power Sources, 2014, 259: 33−42.

[3] TURNER J A. Sustainable hydrogen production [J]. Science, 2004, 305(5686): 972−974.

[4] HSU H C, SHOWN I, WEI H Y, CHANG Y C, DU H Y, LIN Y G, TSENG C A, WANG C H, CHEN L C, LIN Y C. Graphene oxide as a promising photocatalyst for CO_2 to methanol conversion [J]. Nanoscale, 2013, 5(1): 262−268.

[5] CHENG J, ZHANG M, WU G, WANG X, ZHOU J H, CEN K F. Photoelectrocatalytic reduction of CO_2 into chemicals using Pt-modified reduced graphene oxide combined with Pt-modified TiO_2 nanotubes [J]. Environmental Science & Technology, 2014, 48(12): 7076−7084.

[6] GARC A M, AGUIRRE M J, CANZI G, KUBIAK C P, OHLBAUM M, ISAACS M. Electro and photoelectrochemical reduction of carbon dioxide on multimetallic porphyrins/polyoxotungstate modified electrodes [J]. Electrochimica Acta, 2014, 115: 146−154.

[7] SONG J T, IWASAKI T, HATANO M. Photoelectrochemical CO_2 reduction on 3C-SiC photoanode in aqueous solution [J]. Japanese Journal of Applied Physics, 2015, 54(4S): 04DR05.

[8] CHAUDHARY Y S, WOOLERTON T W, ALLEN C S, WARNER J H, PIERCE E, RAGSDALE S W, ARMSTRONG F A. Visible light-driven CO_2 reduction by enzyme coupled CdS nanocrystals [J]. Chemical Communications, 2012, 48(1): 58−60.

[9] HASAN M R, HAMID S B A, BASIRUN W J. Charge transfer behavior of graphene-titania photoanode in CO_2 photo-electrocatalysis process [J]. Applied Surface Science, 2015, 339: 22−27.

[10] LEI Z, LIAN J S. Effect of substrate temperature on structural properties and photocatalytic activity of TiO_2 thin films [J]. Transactions of Nonferrous Metals Society of China, 2007, 17(4): 772−776.

[11] CHEN W, HUA D, TIAN J Y, ZHANG J M. Photocatalytic activity enhancing for TiO_2 photocatalyst by doping with La [J]. Transactions of Nonferrous Metals Society of China, 2006, 16: s728−s731.

[12] ZHANG K J, WEI X, LI X J, ZHENG S J, GANG X, WANG J H. Photocatalytic oxidation activity of titanium dioxide film enhanced by Mn non-uniform doping [J]. Transactions of Nonferrous Metals Society of China, 2006, 16(5): 1069−1075.

[13] JUN D, XIN G, QI W, JIAO L, GUO H Z, ZOU J G. Hydrophilic and photocatalytic activities of Nd-doped titanium dioxide thin films [J]. Transactions of Nonferrous Metals Society of China, 2015, 25(8): 2601−2607.

[14] LIANG J S, MENG J P, LIANG G C, FENG Y W, YAN D. Preparation and photocatalytic activity of composite films containing clustered TiO_2 particles and mineral tourmaline powders [J]. Transactions of Nonferrous Metals Society of China, 2006, 16: s542−s546.

[15] LI Y Y, HAO H S, WANG L J, GUO W H, QING S, LEI Q, GAO W Y, LIU G S, HU Z Q. Preparation and photoelectric properties of Ho^{3+}-doped titanium dioxide nanowire downconversion photoanode [J]. Transactions of Nonferrous Metals Society of China, 2015, 25(12): 3974−3979.

[16] LIU C J, YANG Y H, LI W Z, LI J, LI Y M, CHEN Q Y. A novel Bi_2S_3 nanowire@TiO_2 nanorod heterogeneous nanostructure for photoelectrochemical hydrogen generation [J]. Chemical Engineering Journal, 2016, 302: 717−724.

[17] TONG H X, CHEN Q Y, YIN Z L, HU H P, LI J, LI Z. Preparation of TiO_2 photocatalyst coated with WO_3 for O_2 evolution [J]. Transactions of Nonferrous Metals Society of China, 2008, 18(4): 682−687.

[18] TONG H X, CHEN Q Y, ZHAO L, WU D X, YANG D W. Photo-catalytic behavior of WO_3−TiO_2 catalysts with oxygen evolution [J]. Integrated Ferroelectrics, 2011, 127(1): 63−70.

[19] LI W Z, JIN G H, HU H S, LI J, YANG Y H, CHEN Q Y. Phosphotungstic acid and WO_3 incorporated TiO_2 thin films as novel photoanodes in dye-sensitized solar cells [J]. Electrochimica Acta, 2015, 153: 499−507.

[20] GEROSA M, DI VALENTIN C, ONIDA G, BOTTANI C E, PACCHIONI G. Anisotropic effects of oxygen vacancies on electrochromic properties and conductivity of γ-monoclinic WO_3 [J]. The Journal of Physical Chemistry C, 2016, 120(21): 11716−11726.

[21] DUNNILL C W, NOIMARK S, PARKIN I P. Silver loaded WO_{3-x}/TiO_2 composite multifunctional thin films [J]. Thin Solid Films, 2012, 520(17): 5516−5520.

[22] WANG K, SHI Y T, DONG Q S, LI Y, WANG S F, YU X F, WU M Y, MA T L. Low-temperature and solution-processed amorphous WO_x as electron-selective layer for perovskite solar cells [J]. The Journal of Physical Chemistry Letters, 2015, 6(5): 755−759.

[23] VASILOPOULOU M, SOULTATI A, GEORGIADOU D, STERGIOPOULOS T, PALILIS L, KENNOU S, STATHOPOULOS N, DAVAZOGLOU D, ARGITIS P. Hydrogenated under-stoichiometric tungsten oxide anode interlayers for efficient and stable organic photovoltaics [J]. Journal of Materials Chemistry A, 2014, 2(6): 1738−1749.

[24] LIU Y, LI J, LI W Z, LIU Q, YANG Y H, LI Y M, CHEN Q Y. Enhanced photoelectrochemical performance of WO_3 film with HfO_2 passivation layer [J]. International Journal of Hydrogen Energy, 2015, 40(29): 8856−8863.

[25] JIONG L D. A determination on the index of oxygen in blue tungsten oxide [J]. China Tungsten Industry, 2000, 15(2): 32−33. (in Chinese)

[26] CHUN T A, XI W E, QIANG Z Z. Accurate measurement of oxygen index of tungsten oxides and tungsten bronzes [J]. Powder Metallurgy Technology, 1984(2): 43−47. (in Chinese)

[27] PENG L Z. On determination of non-stoichiometic ratio between tungsten and oxygen in blue tungsten oxide [J]. Chinese Journal of Analysis Laboratory, 1986, 5(10): 1−5. (in Chinese)

[28] LIU Y, LI J, LI W Z, YANG Y H, LI Y M, CHEN Q Y. Enhancement

of the photoelectrochemical performance of WO_3 vertical arrays film for solar water splitting by gadolinium doping [J]. The Journal of Physical Chemistry C, 2015, 119(27): 14834−14842.

[29] SHPAK A P, KORDUBAN A M, MEDVEDSKIJ M M, KANDYBA V O. XPS studies of active elements surface of gas sensors based on WO_{3-x} nanoparticles [J]. Journal of Electron Spectroscopy and Related Phenomena, 2007, 156−158: 172−175.

[30] LIU Y, LI J, TANG H, LI W Z, YANG Y H, LI Y M, CHEN Q Y. Enhanced photoelectrochemical performance of plate-like WO_3 induced by surface oxygen vacancies [J]. Electrochemistry Communications, 2016, 68: 81−85.

[31] KHARE C, SLIOZBERG K, MEYER R, SAVAN A, SCHUHMANN W, LUDWIG A. Layered WO_3/TiO_2 nanostructures with enhanced photocurrent densities [J]. International Journal of Hydrogen Energy, 2013, 38(36): 15954−15964.

[32] ZHU J, LI W Z, LI J, LI Y M, HU H S, YANG Y H. Photoelectrochemical activity of $NiWO_4/WO_3$ heterojunction photoanode under visible light irradiation [J]. Electrochimica Acta, 2013, 112: 191−198.

[33] YANG J, LI W Z, LI J, SUN D B, CHEN Q Y. Hydrothermal synthesis and photoelectrochemical properties of vertically aligned tungsten trioxide (hydrate) plate-like arrays fabricated directly on FTO substrates [J]. Journal of Materials Chemistry, 2012, 22(34): 17744−17752.

[34] LIU C J, YANG Y H, LI W Z, LI J, LI Y M, SHI Q L, CHEN Q Y. Highly efficient photoelectrochemical hydrogen generation using $Zn_xBi_2S_{3+x}$ sensitized platelike WO_3 photoelectrodes [J]. ACS Applied Materials & Interfaces, 2015, 7(20): 10763−10770.

新型 WO_{3-x}/TiO_2 薄膜光阳极光电催化还原 CO_2 制备甲酸

杨亚辉[1]，解人瑞[1]，黎 航[1]，刘灿军[2]，刘文华[2]，占发琦[2]

1. 湖南农业大学 资源与环境学院，长沙 410128；
2. 中南大学 化学化工学院，长沙 410083

摘 要：采用刮涂法制备一种新型光阳极 WO_{3-x}/TiO_2 薄膜，并对其进行光电催化还原 CO_2 制备甲酸。运用 X 射线衍射(XRD)、扫描电镜(SEM)和透射电镜(TEM)对光阳极薄膜进行表征。通过 XPS 确认 WO_{3-x} 中存在氧空位，并通过电位滴定法精确测定 WO_{3-x} 中的氧指数。光电催化还原 CO_2 3 h 后，WO_{3-x}/TiO_2 薄膜光阳极的甲酸产量为 872 nmol/cm^2，是 WO_3/TiO_2 薄膜光阳极的 1.83 倍。光电化学测试表明，由于氧空位的存在提高材料电荷传输性能，从而提高光电催化还原 CO_2 活性，故 WO_{3-x}/TiO_2 薄膜光阳极相对 WO_3/TiO_2 具有更好的光电催化还原活性。

关键词：光电催化还原；CO_2；甲酸；WO_{3-x}；TiO_2；薄膜光阳极

(Edited by Sai-qian YUAN)